ibid., **105,** 502 (1983).
5. (a) J. S. Jaworski, E. Lesniewska, and M. K. Kalinowski, *J. Electroanal. Chem.*, **105,** 329 (1979); (b) J. S. Jaworski, *ibid.*, **219,** 209 (1987); (c) J. S. Jaworski, *Electrochim. Acta*, **31,** 85 (1986).
6. J. S. Jaworski and M. K. Kalinowski, *J. Electroanal. Chem.*, **76,** 301 (1977).
7. J. H. Wilford and M. D. Archer, *ibid.*, **190,** 271 (1985).
8. F. Ammar and J. M. Savéant, *ibid.*, **47,** 115 (1973).
9. (a) T. Kubota, B. Uno, Y. Matsuhisa, H. Miyazaki, and K. Kano, *Chem. Pharm. Bull.*, **31,** 373 (1983); (b) *ibid.*, **32,** 1 (1984); (c) *ibid.*, **33,** 5155 (1985).
10. J. E. J. Schmitz and J. G. M. van der Linden, *Inorg. Chem.*, **23,** 117 (1984).
11. C. Rüssel and W. Jaenicke, *J. Electroanal. Chem.*, **199,** 139 (1986).
12. M. E. Peover, *Trans. Faraday Soc.*, **58,** 2370 (1962).
13. M. E. Peover, *J. Chem. Soc.*, **82,** 4540 (1962).
14. A. Streitwieser, Jr., "Molecular Orbital Theory for Organic Chemists," Chap. 7, Wiley, New York (1961).
15. E. S. Pysh and N. C. Yang, *J. Am. Chem. Soc.*, **85,** 2124 (1963).
16. H. Shalev and D. H. Evans, *ibid.*, **111,** 2667 (1989).
17. J. A. Pople and D. L. Boveridge, "Approximate Molecular Orbital Theory," McGraw-Hill, Inc., New York (1970).
18. T. Fujinaga, K. Izutsu, and T. Nomura, *J. Electroanal. Chem.*, **29,** 203 (1979).
19. B. G. Cox, G. R. Hedwig, A. J. Parker, and D. W. Watts, *Aust. J. Chem.*, **27,** 477 (1974).

Electrocatalytic Oxidation of Formic Acid and Methanol at the Amorphous $Pt_{66}Sb_{34}$ Electrode

S. G. Sun[1] **and J. Lipkowski***

Department of Chemistry, University of Guelph, Guelph, Ontario, Canada N1G 2W1

Z. Altounian

Physics Department, McGill University, Montreal, Quebec, Canada H3A 2T8

ABSTRACT

The electrocatalytic activity of $Pt_{66}Sb_{34}$ rapidly quenched alloy (glassy metal) towards oxidation of HCOOH and CH_3OH has been investigated. The studies have been carried out in an apparatus in which combined surface analysis electrochemistry experiments can be performed. The electrodes were cleaned by standard UHV procedures, and their surface composition was analyzed using Auger electron spectroscopy before each electrochemical experiment. The electrocatalytic activity of the material has been directly correlated with the surface composition of the alloy. The rapidly quenched $Pt_{66}Sb_{34}$ is a single-phase alloy of homogeneous composition, free from grain boundaries. No surface segregation or leaching of alloy elements were observed during experiments which lasted several hours. Its surface composition displayed a long term stability. The rate of CH_3OH and HCOOH oxidation at this material is about 5 to 20 times higher than that at a pure, smooth, polyoriented Pt electrode. It has been shown that the enhanced catalytic activity of the glassy alloy is a complex function of electronic, geometric, and synergistic effects.

The small organic molecules such as methanol or formic acid could be easily oxidized on platinum electrodes and hence constitute potential fuels for direct fuel cells. The oxidation of these compounds involves a surface reaction between an adsorbed organic molecule (or fragment of the organic molecule) and adsorbed oxygen or hydroxyl radical [for review see (1)]. It is well established that electrooxidation of HCOOH and CH_3OH proceeds at a higher rate at surfaces of binary alloys of Pt or at Pt surface modified by submonolayer deposition of foreign metal adatoms (2-12). However, practical use of the binary catalysts is restricted by a number of limitations. The platinum electrodes modified by submonolayer deposition of foreign metal adatoms are not stable (3, 11-15). The crystalline alloys are often multiphase systems having interphase and intergrain boundaries, consequently the distribution of the elements across the alloy surface is not uniform. In addition, surface segregation and miscibility gaps in the phase diagrams often impede attempts to change the catalyst activity by changing the alloy composition.

In principle, the thermodynamic constraints imposed by miscibility gaps and surface segregation can be overcome by rapid quenching of alloys from the liquid phase at a quenching rate higher than the crystallization rate. The rapidly quenched metals are single-phase alloys which display a random distribution of atoms in the binary mixture. They resemble a supercooled liquid, hence, they are frequently called "glassy metals." Our previous experiments on vitreous Pt electrodes (16-18) have shown that their electrocatalytic properties are quite similar to the properties of Pt electrodes modified by a submonolayer of foreign adatoms. In contrast to adatom modified surfaces, the surface composition of glassy metals displays long term stability and therefore they are much better candidates for electrocatalysts in fuel cells.

This is the third paper in a series (17, 18) devoted to systematic studies of electrocatalytic activities of vitreous binary alloys of platinum. This work describes concerted investigations of the surface composition and the kinetics of electrochemical oxidation of formic acid and methanol at the amorphous $Pt_{66}Sb_{34}$ alloy. The studies have been performed in an apparatus built for combined surface analysis/electrochemistry experiments. The instrument allows fast transfer in a period of about 10 min of a sample from an electrochemical cell housed in a controlled environment chamber to the ultrahigh vacuum (UHV) chamber for surface study. In this way the electrocatalytic activity of the alloy has been related to the known composition of its surface.

Experimental

Preparation of the amorphous $Pt_{66}Sb_{34}$ alloy has been described in an earlier contribution (18). The composition of the alloy corresponded to the deep eutectic point in the phase diagram, the x-ray diffraction pattern showed broad peaks and a total absence of sharp lines indicating excellent amorphicity of the material. The crystallization temperature, T_c, determined using differential scanning calorimetry is equal to 540 K. The alloy displays excellent long term stability at room temperature.

The surface analysis of the samples was carried out in the UHV apparatus which will be described in detail in a separate publication (19). Before each measurement, the

* Electrochemical Society Active Member.
[1] On leave from the Department of Chemistry, University of Xiamen, Xiamen, Fujian, China.

surface of the amorphous $Pt_{66}Sb_{34}$ alloy was cleaned by Ar plasma bombardment at argon pressure equal to 2×10^{-5} torr, beam energy equal to 3 keV and the current at the sample adjusted between 1 and 2 μA. The Auger electron spectra were recorded using a Varian 981-2601 cylindrical mirror analyzer (CMA) equipped with a Varian 981-2745 integral electron gun, at a primary beam current of 1 μA and a beam energy of 3 keV. The elemental surface composition of the alloy was determined using the formula

$$C_x = \frac{I_x/S_x}{\sum_\alpha I_\alpha/S_\alpha} \quad [1]$$

where C_x is the atomic concentration of element x in the sample, I_x or I_α is the peak-to-peak amplitude of the Auger signal for element x or α corrected for the scale factor, S_x or S_α is the relative sensitivity between element x or α and silver taken from Ref. (20). The vacuum was generally maintained at 2×10^{-9} torr during the experiments.

The electrochemical measurements concerning the amorphous $Pt_{66}Sb_{34}$ alloy were carried out under 1 atm of argon in a controlled environment chamber attached to the UHV chamber. The controlled environment chamber housed an all-glass electrochemical cell connected by a Teflon tube to a manifold which allowed the cell to be filled with the investigated solution or washed with water. The cell was equipped with a Pt coil counterelectrode and a palladium wire saturated with hydrogen as reference electrode (in the presentation of results the potentials were recalculated and presented in a reversible hydrogen reference electrode scale, HRE). The 0.1*M* $HClO_4$ solution used as the electrolyte was prepared from suprapure 65% perchloric acid (Seastar Chemicals) and Milli-Q water (17 MΩ · cm).

Results

Characterization of the amorphous $Pt_{66}Sb_{34}$/electrolyte interface.—The ribbon-shaped sample of the vitreous $Pt_{66}Sb_{34}$ alloy was cleaned from impurities by Ar^+ bombardment in the UHV chamber. Spectrum a in Fig. 1 shows the Auger spectrum of the sample cleaned by 30 min of sputtering by Ar^+ ions (3 keV energy, 1 μA beam current). The Sb atoms are preferentially sputtered by Ar^+, hence, the alloy surface became enriched in Pt for prolonged Ar^+ bombardment. The surface composition of the sample whose spectrum is shown in Fig. 1a corresponds to 81% Pt and 16% Sb (3% C as impurities). Samples of this surface composition could be obtained reproducibly, and therefore all experiments were performed on such prepared electrodes. To avoid confusion we will always refer to the alloy using its bulk composition. However, the reader is reminded that due to the sample pretreatment its surface is enriched in Pt and surface concentration of Sb atoms is only 16%. The surface of the ribbon was rough, and hence it was difficult to remove carbon impurities even by a long Ar^+ sputtering. The ribbon characterized by this spectrum was subsequently transferred to the controlled environment chamber for electrochemical studies. The cyclic voltammogram (CV) obtained for clean amorphous $Pt_{66}Sb_{34}$ in 0.1*M* $HClO_4$ solution is shown in Fig. 2a. For comparison the cyclic voltammetry curve obtained for pure polyoriented Pt is shown in Fig. 2b as well. The two peaks observed on the CV for $Pt_{66}Sb_{34}$ at 0.14 and 0.27V correspond, apparently, to hydrogen adsorption/desorption at the sites provided by Pt atoms present at the surface. It was assumed that the charge density for hydrogen adsorption corresponded to 210 μC · cm^{-2}. The active area for the $Pt_{66}Sb_{34}$ was then determined from the ratio of the charge of hydrogen adsorption to the value of 210 μC · cm^{-2}. We arbitrarily assumed that charge density for hydrogen adsorption at $Pt_{66}Sb_{34}$ alloy is equal to the charge density for hydrogen adsorption at polycrystalline Pt. Since the surface composition of Sb atoms was only 16% such assumption should lead to an error of the order of 16%. This figure is small in comparison with the magnitude of the electrocatalytic effect reported in this paper.

The sections of the CVs corresponding to potentials more positive than 0.5V were distinctly different between the $Pt_{66}Sb_{34}$ alloy and the polyoriented Pt electrode. The reversible peak at 0.65V and a shoulder at 0.70V observed at the glassy metal electrode have approximately the same position as the peaks observed on polyoriented Pt modified by the submonolayer deposition of Sb atoms (18). Consequently, the peaks can be identified as corresponding to oxygen adsorption on Sb atoms present at the surface. The multiple potential cycles applied to the glassy metal electrode had no effect on the shape of the curve as long as the positive potential limit was lower than 1.0 V/RHE. When

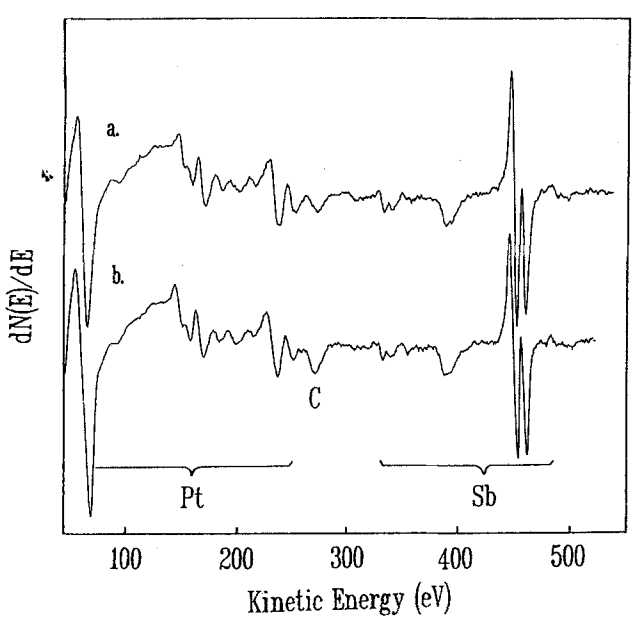

Fig. 1. Auger spectra of amorphous $Pt_{66}Sb_{34}$ alloy. a, Clean surface obtained after 30 min. of Ar^+ sputtering; b, surface emersed from 0.1*M* $HClO_4$ solution after completion of electrochemical experiment shown in Fig. 2a.

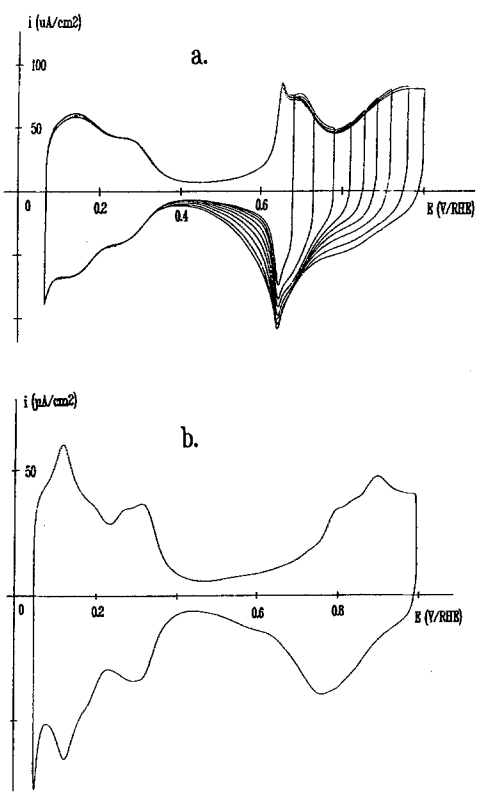

Fig. 2. Cyclic voltammograms obtained in 0.1*M* $HClO_4$ solution with sweep rate of 50 mV · s^{-1}. (a) Amorphous $Pt_{66}Sb_{34}$ alloy, with progressive increase of upper limit of the reverse potential from 0.68 to 1.0 V/RHE; (b) polyoriented Pt electrode after cleaning by flaming and quenching procedure.

the sample was emersed from the electrolyte solution, cleaned with ultrapure water, and transferred back into the UHV chamber, it displayed an Auger spectrum (Fig. 1b) which is practically identical to spectrum a in Fig. 1. Therefore, polarization of the alloy surface up to a potential of 1.0 V/RHE had no effect on the surface composition.

Electrocatalytic oxidation of HCOOH.—The kinetics of HCOOH oxidation were initially investigated using cyclic voltammetry. The clean sample of the amorphous $Pt_{66}Sb_{34}$ alloy (surface composition 81% Pt, 16% Sb, and 3% C impurities) was transferred to the controlled environment chamber and immersed into a solution of 0.1*M* $HClO_4$ and 0.1*M* HCOOH at 0.2 V/RHE, and the cyclic voltammetry curves were recorded. Figure 3a shows the CVs determined for HCOOH oxidation on the glassy metal electrode. For comparison, the cyclic voltammetry curves determined at the pure polyoriented Pt is shown in Fig. 3b. The differences between the two curves are apparent. Multiple potential cycles applied to the glassy metal electrode have little effect on the magnitude of the voltammetric current. In contrast the current of HCOOH oxidation at the pure polyoriented Pt dramatically decreases with the number of potential cycles applied. For example the magnitude of the peak observed at a potential of about 0.8V in the negative going potential sweep decreased by a factor of 6 during 19 min of continuous potential cycling. Figure 3 shows also that in the potential region between 0.4 and 0.8 V/RHE, the oxidation currents corresponding to the potential sweep in the positive going direction are much higher at the vitreous electrode than that at the polyoriented Pt.

In order to study the kinetics of HCOOH oxidation in greater detail, potential step experiments were performed using the program shown in Fig. 4. The electrode potential was initially held at E_i = 0.2V for a period of 14.5s, long enough to establish adsorption equilibrium between the electrode surface and the bulk of the solution, and then

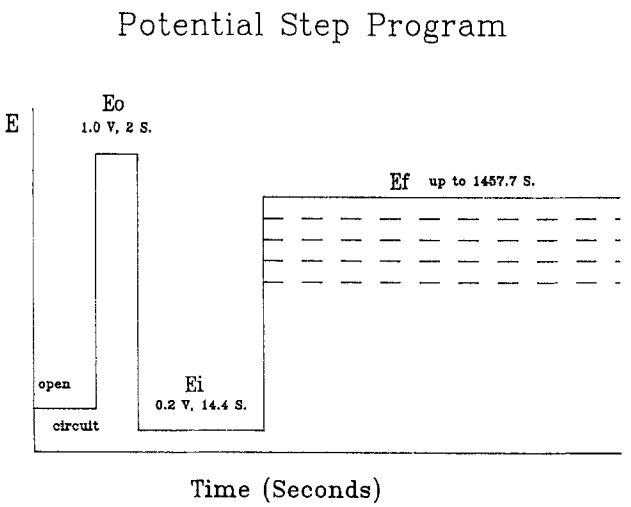

Fig. 4. Potential program applied to the investigated electrode during the potential step experiments.

was stepped to E_f, more positive than E_i, and the chronoamperometric transients were recorded over a period of 1457.7s. Then the cell was turned off for transfer of the data from the potentiostat to the computer. To perform another experiment the potential was first stepped to E_o = 1.0 V/RHE, to oxidize organic impurities and/or poisoning intermediates accumulated during the long electrolysis at E_f, and after 2s returned to E_i. The same experiment was repeated for E_f values ranging from 0.45 to 1.0 V/RHE while the values of E_i and E_o were kept constant.

Representative current transients obtained in the potential step experiments are presented as the three-dimensional *i-t-E* plot in Fig. 5. Because the current transients were acquired in a time window which covers three decades, the time axis in Fig. 5 has a logarithmic scale. At the

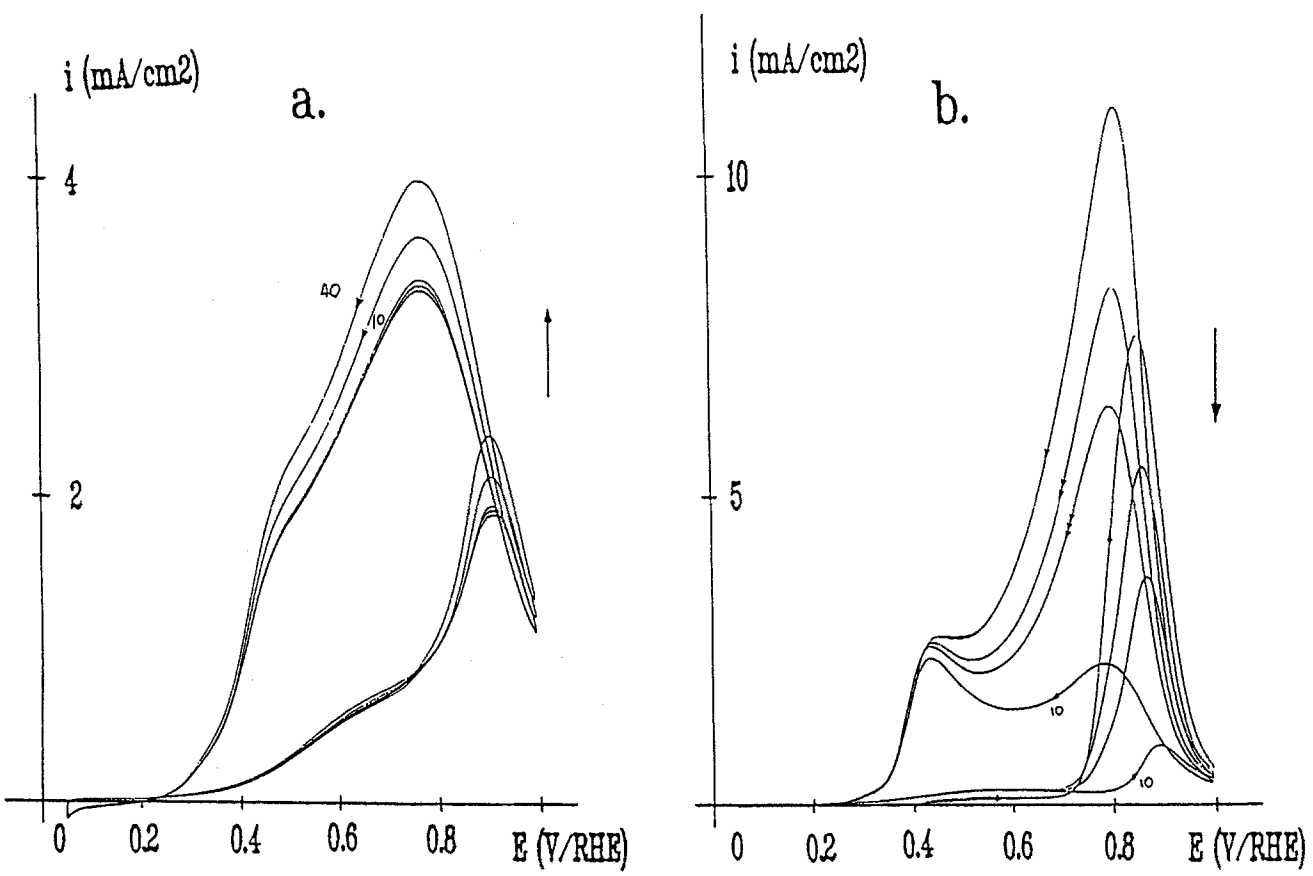

Fig. 3. Cyclic voltammetric curves obtained in 0.1M $HClO_4$ + 0.1M HCOOH solution with sweep rate of 50 mV · s^{-1}. (a) Amorphous $Pt_{66}Sb_{34}$ alloy electrode, the curves obtained in 10th and 40th cycle are indicated in the figure, respectively; (b) polyoriented Pt electrode, the curves obtained in 1st (—>—), 2nd (—>—>—), 3rd (—>—>—>—) and 10th cycle are indicated in the figure.

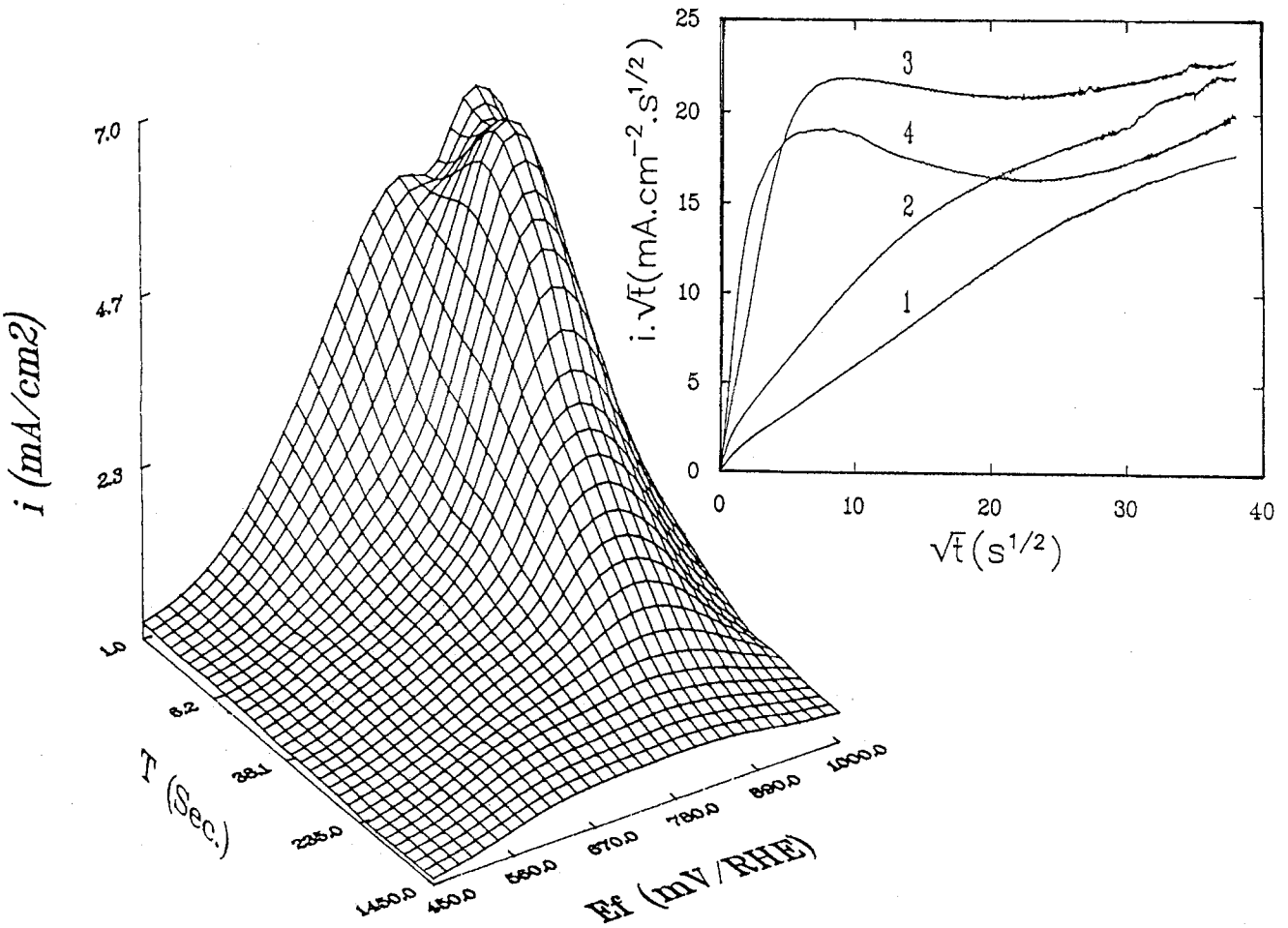

Fig. 5. Three-dimensional plots of the current transients obtained over the whole range of E_f investigated on the amorphous $Pt_{66}Sb_{34}$ electrode in 0.1M $HClO_4$ + 0.1M HCOOH solution. Note that the time axis has a logarithmic scale. Insert: plot of $i\sqrt{t}$ vs. $\sqrt{t}$ for a few selected E_f: curve 1, 0.6, curve 2, 0.7, curve 3, 0.8, and curve 4, 0.9 V/RHE.

end of the HCOOH oxidation experiment, the sample was emersed from the investigated solution then immersed again in 0.1*M* $HClO_4$ to oxidize the adsorbed HCOOH and adsorbed intermediates of the oxidation reaction, washed with ultrapure water, and transferred back into the UHV chamber. The Auger spectrum recorded on a so-treated sample was essentially identical to spectrum b in Fig. 1. The quantitative analysis shows that the differences between the surface concentration of Pt and Sb before and after the experiment are insignificant in comparison with the experimental error. In conclusion, the composition of the alloy surface was not changed during the course of the experiment which lasted several hours.

As Fig. 5 shows, the oxidation currents pass through a maximum as a function of both potential and time. In order to examine the character of the time dependence of the potentiostatic current, the mass transport contribution to the measured current must be evaluated. The electrode had the shape of a very thin ribbon and experiments were carried out in unstirred solutions while all vibrations were effectively damped out. Under such conditions the lower limit of the mass transport controlled current is determined by a linear diffusion. The insert to Fig. 5 shows a plot of the product $i\sqrt{t}$ *vs.* $\sqrt{t}$ calculated for four electrode potentials. For the potential corresponding approximately to the position of maximum on the *i-E* profiles taken at a constant value of t the product $i\sqrt{t}$ rises initially fast and then becomes approximately independent of time. The limiting value of $i\sqrt{t}$ corresponds approximately to 23 mA $\cdot$ cm^2 $\cdot$ s$^{1/2}$. The value of $i\sqrt{t}$ calculated with the help of the Cottrell equation (taking the value of the diffusion coefficient for HCOOH as equal to 5×10^{-6} cm^2 $\cdot$ s$^{-1/2}$) is equal to 256 mA $\cdot$ cm^{-2} $\cdot$ s$^{1/2}$. The difference between the experimental and calculated values of $i\sqrt{t}$ can be fully accounted for by the uncertainty in the determination of the electrode area for $Pt_{66}Sb_{34}$ electrode. Consequently, the data presented in Fig. 5 suggest that for times longer than 20s the rate of HCOOH oxidation at the vitreous PtSb electrode may be controlled by diffusion. However, for such a long time of electrolysis the contribution of the convection to the overall mass transport may not be neglected. The mass transport current may be higher than the value predicted by the Cottrell equation and therefore higher than the observed current of HCOOH oxidation. Nevertheless, the results presented above indicate that at least significant contribution of mass transport to the mechanism of HCOOH oxidation at the PtSb alloy should be expected.

For comparison, the potential step experiments were also performed at the polyoriented Pt electrode, and the corresponding current transients are presented in the three-dimensional coordinates in Fig. 6 (the time axis, as in Fig. 5, has a logarithmic scale). In order to evaluate the mass transport contribution the products $i\sqrt{t}$ were calculated and plotted against $\sqrt{t}$ in the insert to the figure. The polyoriented Pt electrode consisted of a nearly spherical bead of radius 0.1 cm. Linear plots of $i\sqrt{t}$ *vs.* $\sqrt{t}$, giving the intercept of 25 mA $\cdot$ cm^{-2} $\cdot$ s$^{1/2}$ (calculated with the help of the Cottrell equation) were expected for currents controlled by diffusion to the sphere. The plots shown in the insert to Fig. 6 are nonlinear and the experimental values of $i\sqrt{t}$ are much lower than the values of the product calculated for a diffusion controlled reaction. This result indicates that HCOOH oxidation at the polyoriented Pt electrode is primarily controlled by a rate-determining step which involves an interfacial reaction.

The currents of HCOOH oxidation at the glassy metal and the polyoriented electrodes are compared in Fig. 7. The graph shows four cross sections selected from Fig. 5 and 6. Apparently the glassy metal electrode is a much better catalyst of HCOOH oxidation than pure crystalline Pt.

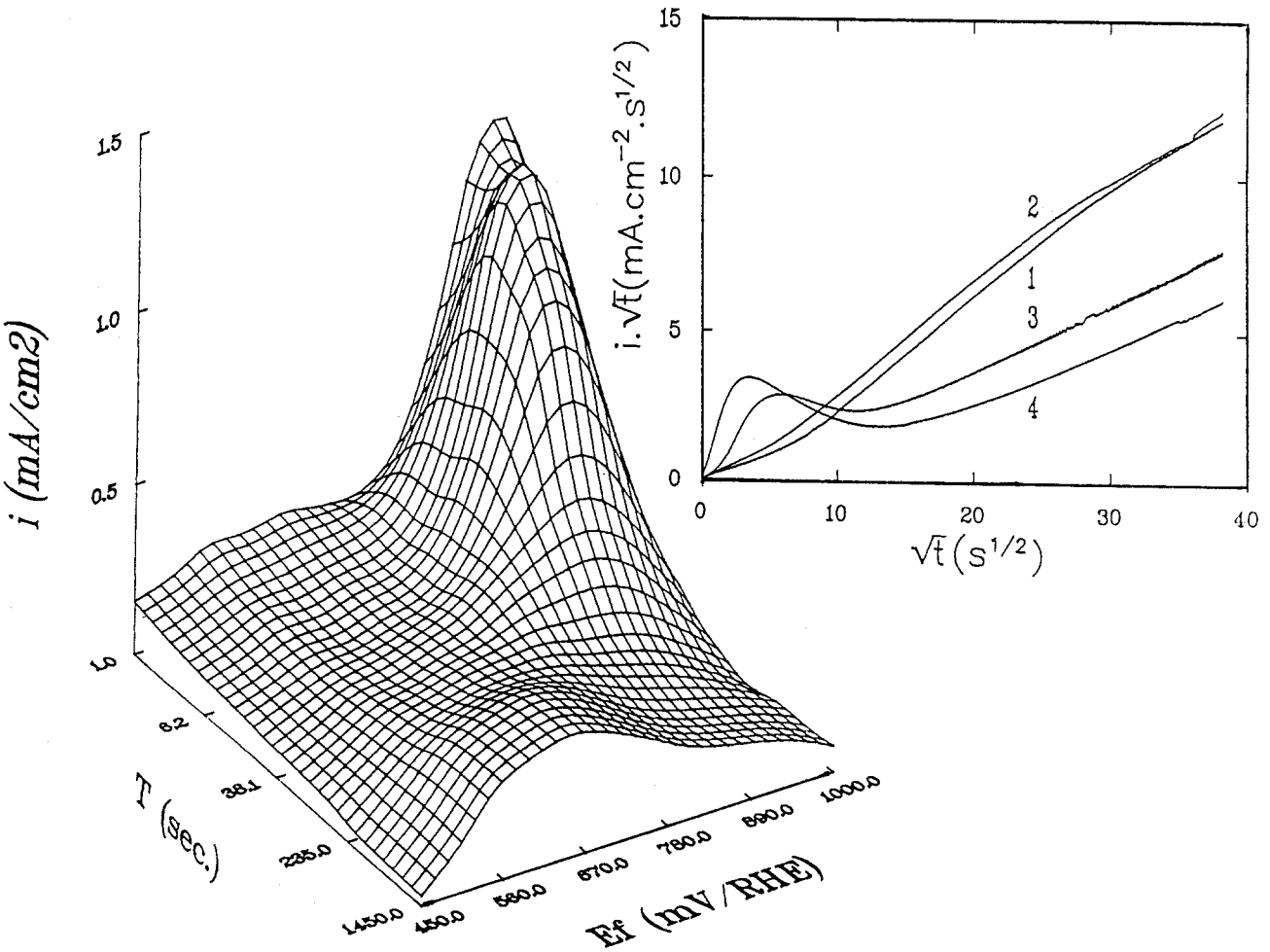

Fig. 6. Three-dimensional plots of the current transients obtained over the whole range of E_f investigated on the polyoriented Pt electrode in 0.1*M* $HClO_4$ + 0.1*M* HCOOH solution. Note that the time axis has a logarithmic scale. Insert is the plot of $i\sqrt{t}$ vs. $\sqrt{t}$ for a few selected E_f: curve 1, 0.6, curve 2, 0.7, curve 3, 0.8, and curve 4, 0.9 V/RHE.

In order to evaluate the effect of the electrode material on the rate of the electrode reaction investigated, the enhancement factor, *R*, defined as the ratio of the oxidation currents measured at the vitreous alloy and pure Pt electrodes, *i.e.*

$$R = \frac{i(Pt_{66}Sb_{34})}{i(Pt)} \qquad [2]$$

was calculated for a few selected potentials. Its values are plotted against the time in the insert to Fig. 7. The time window was restricted to the initial sections of the current transients where the rate of the reaction is controlled by an interfacial process at both electrodes. At very short times the value of *R* apparently changes with time and potential. However for *t* longer than 10s the *R* attains a pseudo "steady-state," potential independent value, approximately equal to 5. In summary, the rate of HCOOH oxidation at the $Pt_{66}Sb_{34}$ electrode proceeds much faster than at pure crystalline Pt.

Oxidation of CH_3OH.—The cyclic voltammetry curves recorded for the clean $Pt_{66}Sb_{34}$ sample transferred from the UHV chamber to the controlled environment chamber and immersed into a solution of 0.1*M* $HClO_4$ and 0.1*M* CH_3OH is shown in Fig. 8. For comparison, the cyclic voltammetry curve determined at the pure polyoriented Pt in the same solution is shown in Fig. 8. The differences between the shape of the voltammetric curves, and between the evolution of the current density with multiple potential cycling, determined for methanol oxidation at $Pt_{66}Sb_{34}$ and that for pure crystalline Pt are similar to the differences observed earlier for HCOOH oxidation at these two electrodes. The shape of CV obtained at $Pt_{66}Sb_{34}$ remains virtually unchanged during the multiple potential sweeps. In contrast, the current density of methanol oxidation on the polyoriented Pt progressively decreases with the number of potential cycles applied to the electrode. Quantitatively, this effect amounts to a fourfold decrease of the peak height during the positive going voltage sweep for a period of 19 min.

As in the studies of HCOOH oxidation, the potential step experiments were performed to investigate quantitatively the kinetics of methanol oxidation. The potential program, shown in Fig. 4 and described above, was employed and the chronoamperometric transients were recorded. The results of methanol oxidation at the amorphous $Pt_{66}Sb_{34}$ electrode are plotted in three-dimensional *i-t-E* coordinates in Fig. 9 (note that the time axis of Fig. 9 has a logarithmic scale). At the end of the experiment the sample was emersed from the solution, washed with water, and transferred to the UHV chamber. The Auger electron spectrum obtained with a so-treated sample showed that the surface composition of the alloy was not changed during the course of the experiment.

Qualitatively, the shape of the three-dimensional plot shown in Fig. 9 is similar to that displayed earlier for HCOOH oxidation in Fig. 5. The currents of methanol oxidation pass through a maximum as a function of both potential and time. In order to evaluate the mass transport contribution to the measured currents, the product $i\sqrt{t}$ was calculated for a few selected potentials and plotted against $\sqrt{t}$ in the insert of Fig. 9. The plots are nonlinear. In addition, the maximum values of $\sqrt{t}$ are about eight times smaller than the value of this product calculated with the help of the Cottrell equation, and assuming that CH_3OH oxidation involves the transfer of six electrons. This result suggests that the mass transport contribution to the meas-

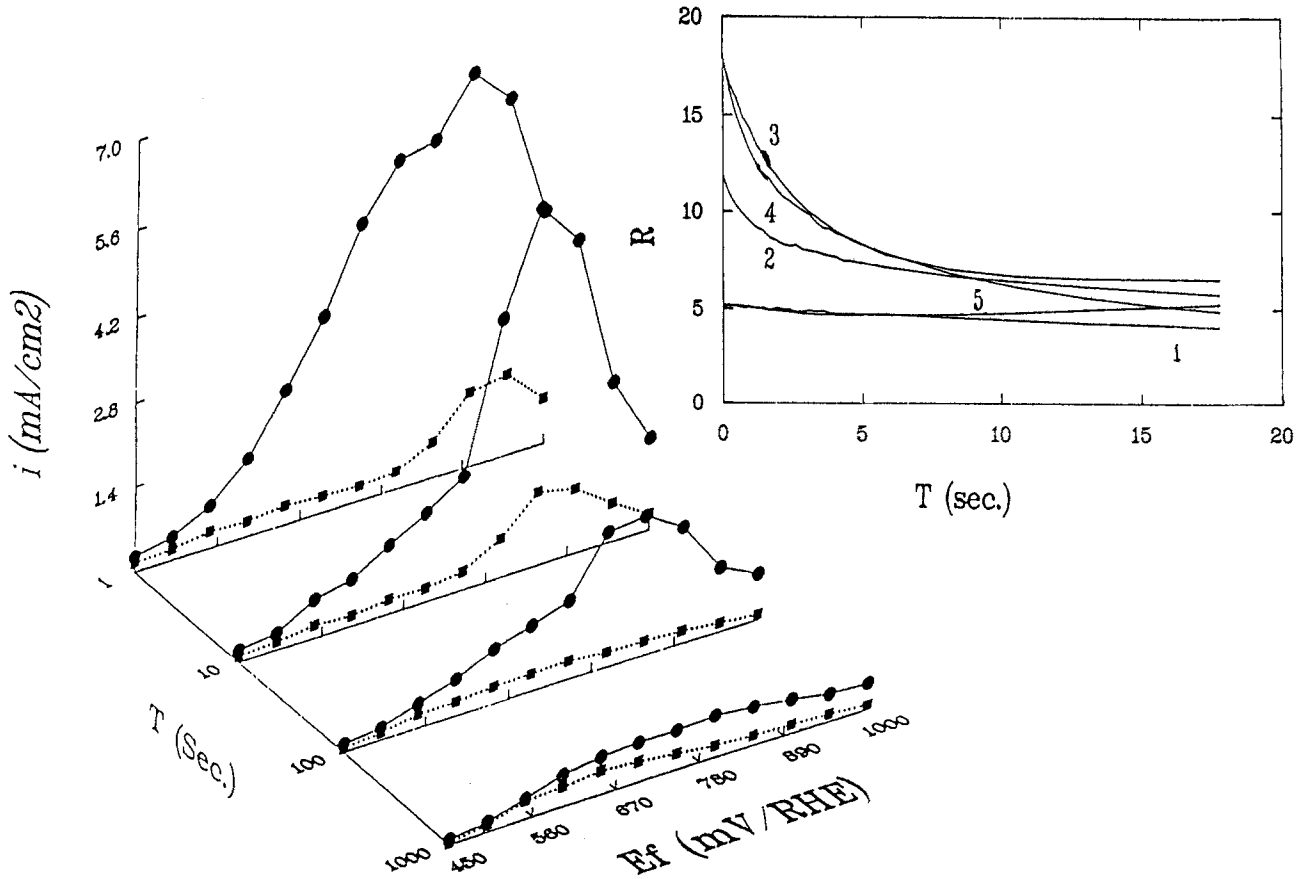

Fig. 7. Comparison of the HCOOH oxidation currents at (●) amorphous $Pt_{66}Sb_{34}$ and at (■) polyoriented Pt electrodes. Insert is the plot of enhancement factor R vs. time for a few selected E_f: curve 1, 0.6, curve 2, 0.7, curve 3, 0.75, curve 4, 0.8, and curve 5, 0.9 V/RHE.

ured currents is negligible and that the rate of methanol oxidation is controlled by an interfacial process.

The chronoamperometric transients determined from the potential step experiments performed at the polyoriented Pt electrode are shown in the three-dimensional coordinates in Fig. 10. The insert to the figure shows a plot of $i\sqrt{t}$ vs. $\sqrt{t}$ obtained for a few selected potentials. The plots are nonlinear, and the products $i\sqrt{t}$ are more than one order of magnitude smaller than the value calculated for a diffusion controlled reaction. Consequently, the rate of CH_3OH oxidation is entirely determined by the rate of an interfacial reaction.

The currents of CH_3OH oxidation at the glassy metal and pure crystalline Pt electrodes are compared in Fig. 11. The data show that the vitreous electrode is much better catalyst of methanol oxidation than pure crystalline Pt. To as-

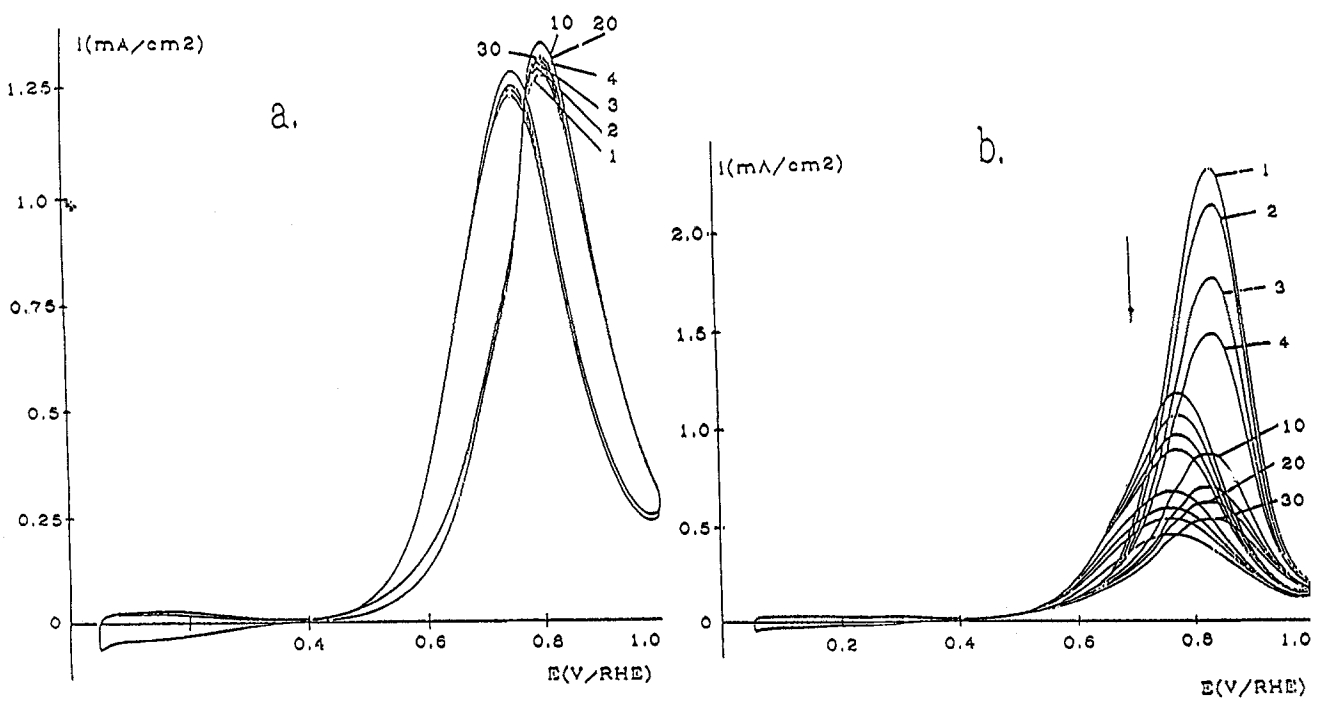

Fig. 8. Cyclic voltammetric curves obtained in 0.1M $HClO_4$ + 0.1M CH_3OH solution with sweep rate at 50 mV · s^{-1}, the curves obtained in 1st, 2nd, 3rd, 4th, 10th, 20th, and 30th cycle are indicated in the figure. (a) Amorphous $Pt_{66}Sb_{34}$ alloy electrode; (b) polyoriented Pt electrode.

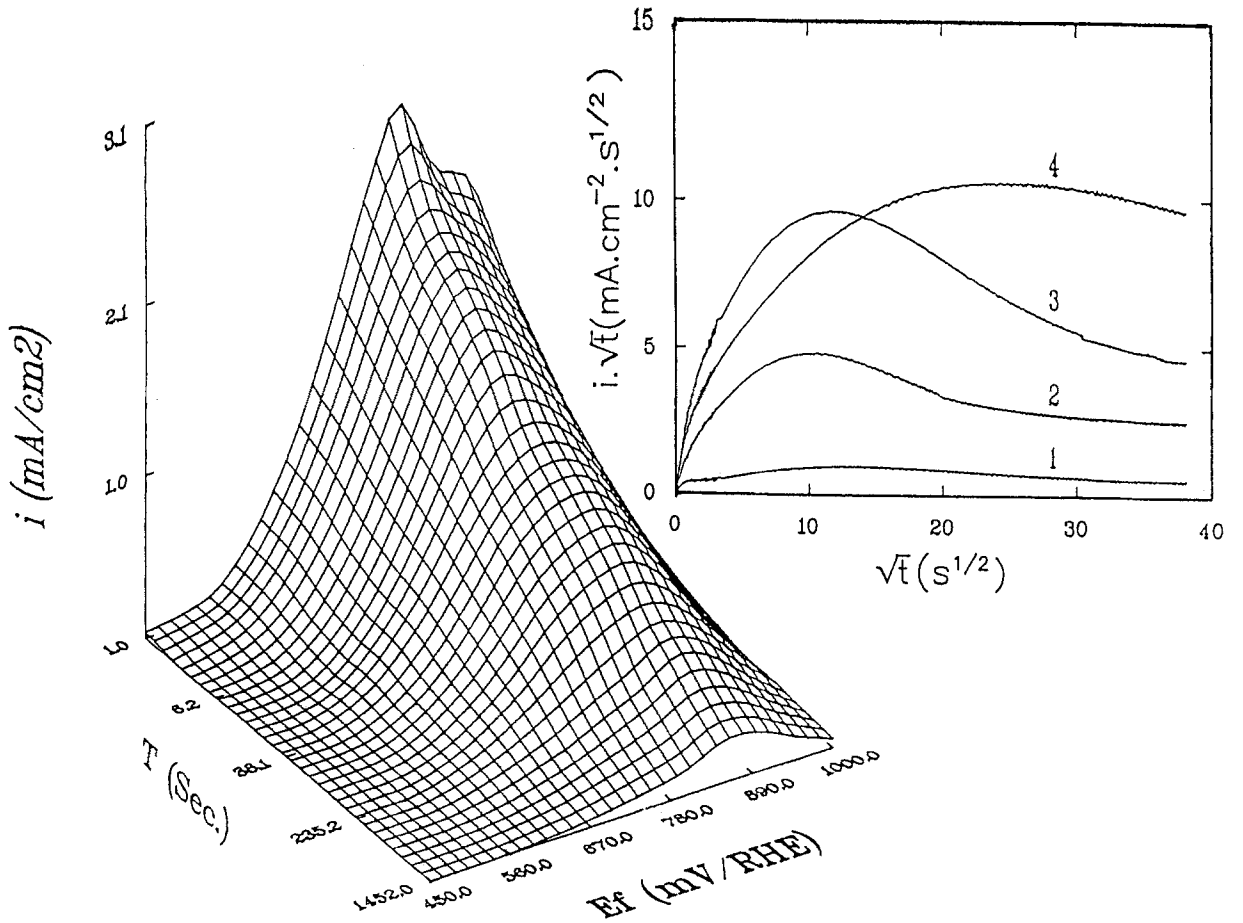

Fig. 9. Three-dimensional plots of the current transients obtained over the whole range of E_f investigated on the amorphous $Pt_{66}Sb_{34}$ electrode in 0.1M $HClO_4$ + 0.1M CH_3OH solution. Note that the time axis has a logarithmic scale. Insert: plot of $i\sqrt{t}$ vs. $\sqrt{t}$ for a few selected E_f: curve 1, 0.6, curve 2, 0.7, curve 3, 0.8, and curve 4, 0.9 V/RHE.

sess quantitatively the effect of the electrode material, the enhancement factor was calculated for a few selected potentials. The results are plotted against time in the insert to Fig. 11. The enhancement factor initially increases with time, passes through a broad maximum, and then slowly decreases. The values of the enhancement factor apparently depend also on the electrode potential. At longer times the values of R for methanol oxidation are higher than the values of R observed earlier for HCOOH oxidation. In conclusion, the results show that the vitreous $Pt_{66}Sb_{34}$ alloy is a very efficient catalyst of methanol oxidation.

Discussion

The results presented above show that the vitreous $Pt_{66}Sb_{34}$ alloy is a significantly better catalyst of the electrochemical oxidation of HCOOH and CH_3OH than pure, smooth, polyoriented platinum. The amorphous state of the alloy ensures homogeneous distribution of its constituents and mixing of Pt with the second element improves the catalytic activity as a result of: (*i*) changes in the electronic structure of the metal due to formation of intermetallic bonds; (*ii*) geometrical effects due to a change in the number and nature of specific adsorption sites which favor the adsorption of organic molecules and the reactive intermediates and block the poision formation reaction; (*iii*) synergistic or bifunctional action when Pt atom adsorbs the reactant molecule and the atom of the second element adsorbs the oxygen which is required to complete the oxidation reaction.

The oxidation of formic acid and methanol are two and six electron reactions, respectively. These processes are generally considered to proceed through a dual pathway mechanism, and may involve a number of intermediates. A simple representation of the reaction mechanism is shown as follows (21, 22)

$$[Pt] + HCOOH\ (or\ CH_3OH) \rightarrow \begin{bmatrix} \rightarrow \text{Reactive Intermediates} \rightarrow \\ \rightarrow \text{Poisoning Intermediates} \rightarrow \end{bmatrix} \rightarrow CO_2 \quad [3]$$

where [Pt] represents the surface platinum sites. The improved activity of the glassy alloy catalyst may result when the channel involving formation of the poisoning intermediates is blocked.

The improvement of the catalytic activity of the glassy alloy electrode is best represented by the magnitude of the enhancement factor R. The data presented above shows that R is a complex function of the reaction time and the electrode potential, this in turn reflects the complex nature of the electrode reactions investigated and shows that both the distribution of the intermediates and the character of the rate-determining steps change with time and potential. Consequently, it is quite likely that not one but a few above-mentioned effects are responsible for improved catalytic activity of the amorphous $Pt_{66}Sb_{34}$. To illustrate this point, the values of the enhancement factor for the oxidation of HCOOH and CH_3OH at short and long times of the experiment were plotted against the electrode potential in Fig. 12 a and c, respectively. Figure 12b shows the charge density of adsorbed oxygen at the amorphous $Pt_{66}Sb_{34}$ and the polyoriented Pt electrodes obtained by the integration of the cyclic voltammetric curves, recorded in solution of supporting electrolyte free from the organic molecules.

The enhancement factor determined for the reaction time equal to 10s is virtually independent of the electrode potential and consequently of the surface coverage by oxygen species. In addition the magnitude of R is approximately the same for both CH_3OH and HCOOH oxidation reactions. These features indicate that enhancement of the catalytic activity of vitreous $Pt_{66}Sb_{34}$ cannot be due to the bifunctional effect. Consequently, for this reaction time the enhanced catalytic activity of the vitreous $Pt_{66}Sb_{34}$ electrode should be primarily due to the electronic and geometric effects.

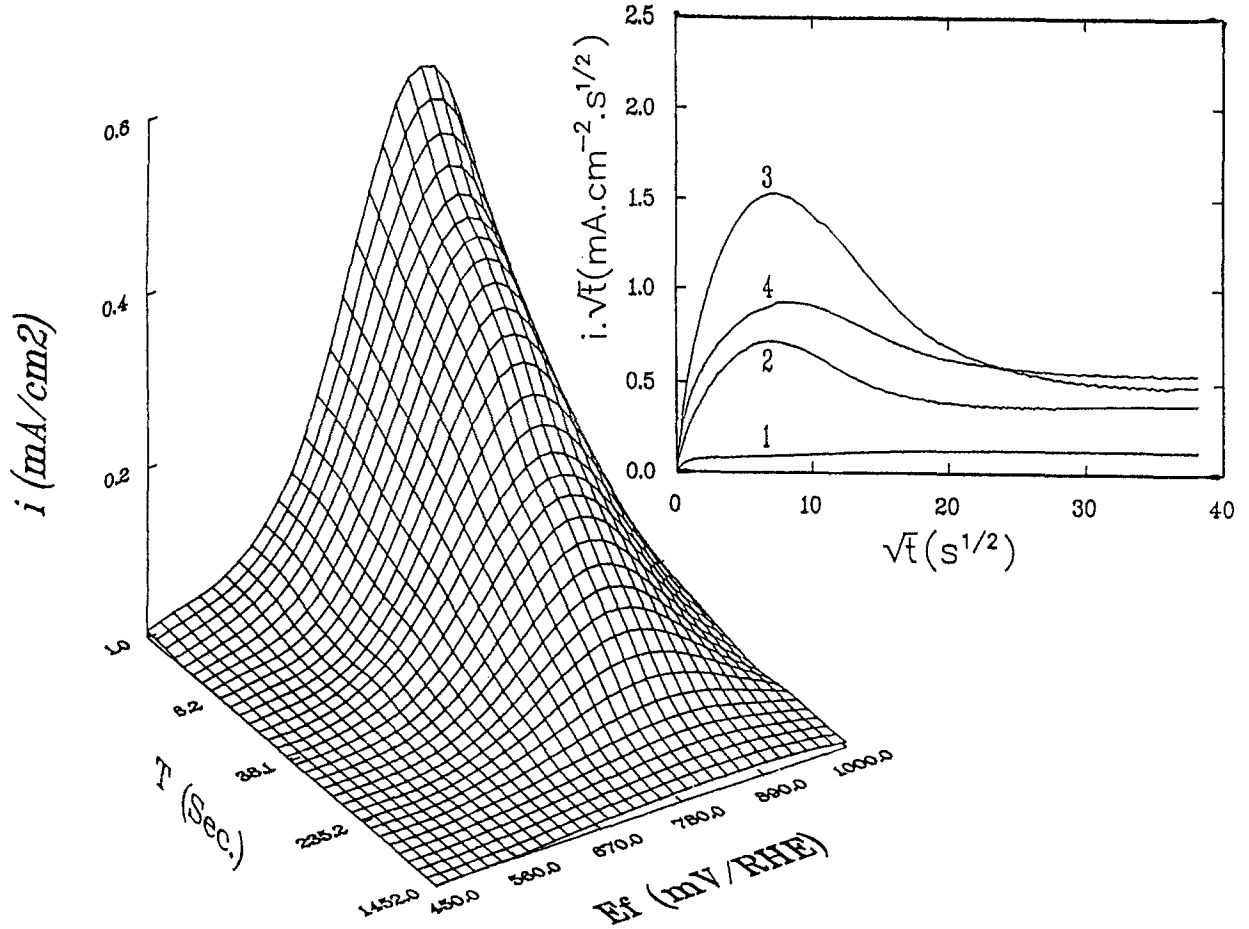

Fig. 10. Three-dimensional plots of the current transients obtained over the whole range of E_f investigated on the polyoriented Pt electrode in 0.1M $HClO_4$ + 0.1M CH_3OH solution. Note that the time axis has a logarithmic scale. Insert is the plot of $i\sqrt{t}$ vs. $\sqrt{t}$ for a few selected E_f: curve 1, 0.6, curve 2, 0.7, curve 3, 0.8, and curve 4, 0.9 V/RHE.

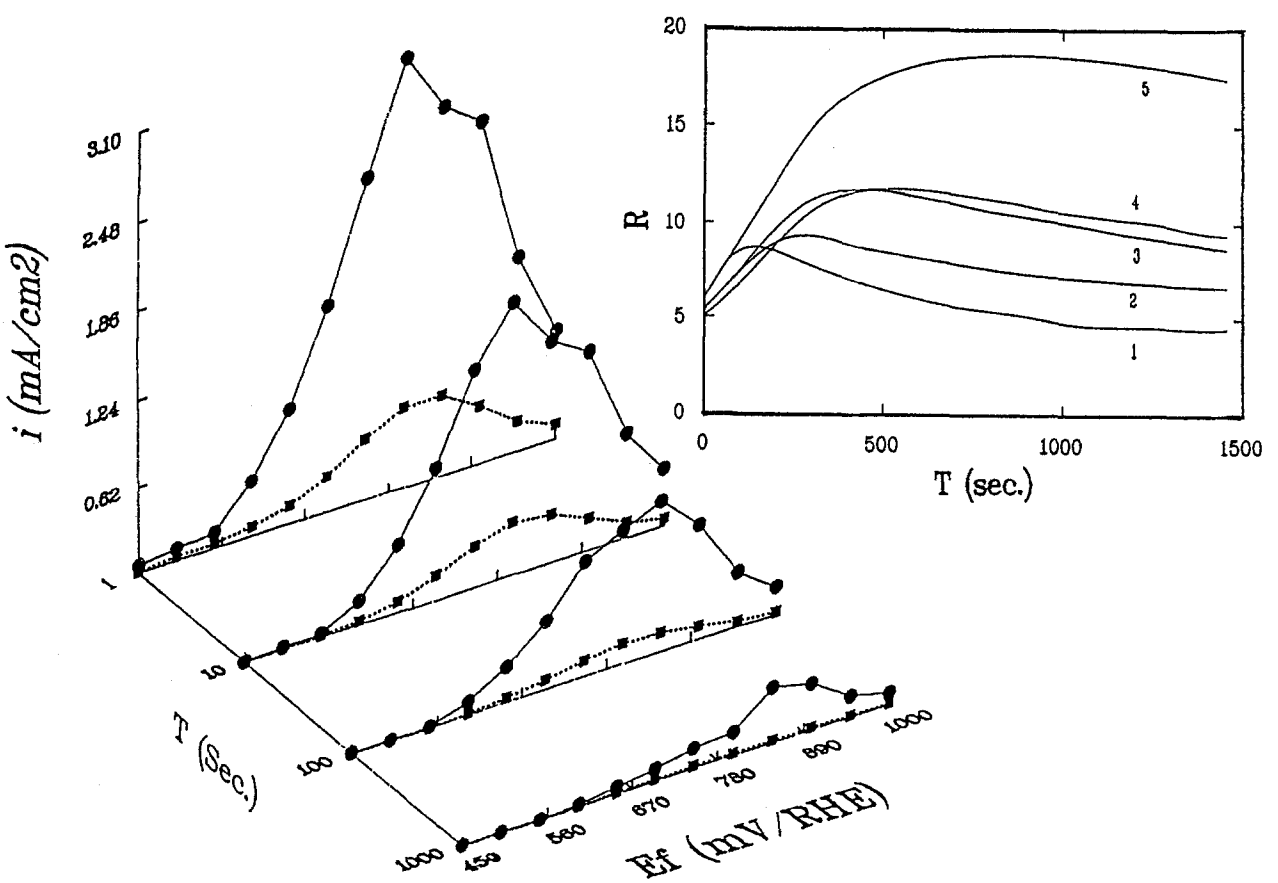

Fig. 11. Comparison of the CH_3OH oxidation currents at (●) amorphous $Pt_{66}Sb_{34}$ and at (■) polyoriented Pt electrodes. Insert is the plot of enhancement factor R vs. time for a few selected E_f: curve 1, 0.6, curve 2, 0.7, curve 3, 0.75, curve 4, 0.8, and curve 5, 0.9 V/RHE.

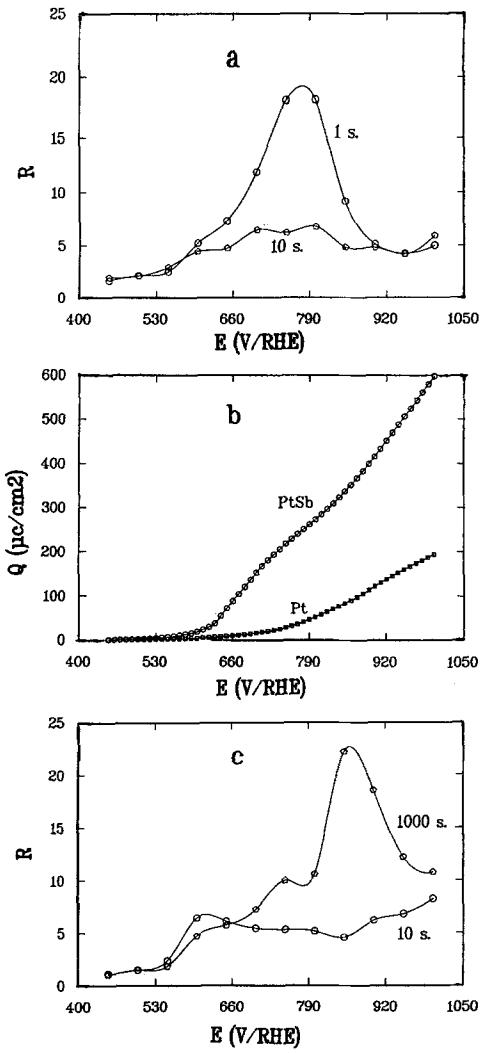

Fig. 12. (a) The enhancement factor *R* for HCOOH oxidation plotted against the electrode potnetial at two selected times of experiment; (b) charge of adsorbed oxygen species obtained by integration of the cyclic voltammetric curves in Fig. 2; (c) the enhancement factor *R* for CH_3OH oxidation plotted against the electrode potential at two selected times of experiment.

In contrast, the 1s curve for HCOOH oxidation and the 1000s curve for $Pt_{66}Sb_{34}$ oxidation display a strong dependence of the enhancement factor on the electrode potential and, in consequence, on the coverage of oxygen species on the electrode surface. Incidentally, the maximum at the 1s curve for HCOOH oxidation coincides with the potential at which the charge of oxygen species adsorbed at Sb atoms attains a quasi-plateau, while the coverage of Pt atoms by oxygen species is still very low. Therefore, it appears, that at the initial stage of HCOOH oxidation, the $Pt_{66}Sb_{34}$ alloy acts as bifunctional catalyst at which HCOOH molecules adsorb at the Pt atoms and react with oxygen or OH radicals absorbed at Sb atoms. The enhancement of $Pt_{66}Sb_{34}$ activity, with respect to CH_3OH oxidation at long reaction times is of a more complex nature. The maximum on the 1000s curve for CH_3OH oxidation, shown in Fig. 12c, corresponds to the potential at which the coverage of Pt sites by adsorbed oxygen species is significant. Consequently, in addition to the bifunctional action of the catalyst, there must be other effects which contribute to the observed magnitude of *R*.

Conclusions

In conclusion, the observed enhancement of the catalytic activity of vitreous $Pt_{66}Sb_{34}$ alloy with respect to oxidation of HCOOH and CH_3OH results from an interplay of a number of effects the most likely of which are changes in the electronic structure of the metal, changes in the number of specific adsorption sites which favor the adsorption of the reactive intermediates, and block the poison formation, bifunctional action which involves adsorption of the organic molecule at Pt atoms, and the oxygen required to complete the oxidation reaction at Sb atoms. The data presented above suggest that the contribution of these effects to the overall catalyst activity vary with potential and reaction time.

Acknowledgment

The authors wish to thank Dr. W. Jedral for his help in the preparation of the computer program used in the potential step experiments. The financial support of the Natural Sciences and Engineering Research Council of Canada through a strategic grant is gratefully acknowledged.

Manuscript submitted Aug. 21, 1989; revised manuscript received Feb. 22, 1990.

The University of Guelph assisted in meeting the publication costs of this article.

REFERENCES

1. R. Parsons and T. Vandernoot, *J. Electroanal. Chem.*, **257,** 9 (1988).
2. R. R. Adzic, in "Advances in Electrochemistry and Electrochemical Engineering," Vol. 13, H. Gerischer and C. W. Tobias, Editors, Wiley, New York (1984).
3. G. Kokkinidis, *J. Electroanal. Chem.*, **201,** 217 (1986).
4. A. Capon and R. Parsons, *ibid.*, **165,** 285 (1975).
5. B. E. Conway, H. Angerstein-Kozlowska, and G. Lzartovyska, *Z. Phys. Chem. N. F.*, **112,** 195 (1978).
6. B. Beden, C. Lamy, and J. M. Leger, *Electrochim. Acta,* **24,** 1157 (1979).
7. N. R. de Tacconi, J. J. Leger, B. Beden, and C. Lamy, *J. Electroanal. Chem.*, **134,** 117 (1982).
8. D. F. A. Koch, D. A. J. Rand, and R. Woods, *ibid.*, **70,** 73 (1976).
9. S. Motoo and M. Watanabe, *ibid.*, **98,** 203 (1985).
10. M. Watanabe, M. Shibata, and S. Motoo, *ibid.*, **187,** 161 (1985).
11. J. Clavilier, A. Fernandez-Vega, J. M. Feliu, and A. Aldaz, *ibid.*, **258,** 89 (1989).
12. A. Fernandez-Vega, J. M. Feliu, A. Aldaz, and J. Clavilier, *ibid.*, **258,** 101 (1989).
13. D. Pletcher and V. Solis, *ibid.*, **131,** 309 (1982).
14. R. W. Tsang, D. C. Johnson, and G. R. Luecke, *This Journal,* **131,** 2369 (1984).
15. T. Vitanov, A. Popov, G. Staikov, E. Budevski, W. J. Lorenz, and E. Schmidt, *Electrochim. Acta,* **31,** 981 (1986).
16. S. G. Sun, D. E. A. Thesis, Paris VI (1983).
17. K. Seto, J. Noël, J. Lipkowski, Z. Altounian, and R. Reeves, *This Journal,* **136,** 1910 (1989).
18. S. G. Sun, J. Noël, J. Lipkowski, and Z. Altounian, *J. Electroanal. Chem.*, **278,** 205 (1990).
19. K. Seto and J. Lipkowski, *ibid.*, In preparation.
20. "Handbook of Auger Electron Spectroscopy," Physical Electronics Division, Perkin-Elmer Corp., Eden Prairie, MN (1976).
21. A. Capon and R. Parsons, *J. Electroanal. Chem.*, **45,** 205 (1973).
22. S. G. Sun, J. Clavilier, and A. Bewick, *ibid.*, **240,** 147 (1988).